

UAB-FT-645
 FERMILAB-PUB-08-152-T
 ANL-HEP-PR-08-32
 EFI-08-15

The Effective Theory of the Light Stop Scenario

M. Carena^a, G. Nardini^b, M. Quirós^{b,c}, C.E.M. Wagner^{d,e}

^a*Theoretical Physics Department, Fermilab, P.O. Box 500, Batavia, IL 60510*

^b*IFAE, Universitat Autònoma de Barcelona, 08193 Bellaterra, Barcelona (Spain)*

^c*Institució Catalana de Recerca i Estudis Avançats (ICREA)*

^d*HEP Division, Argonne National Laboratory, Argonne, IL 60439*

^e*EFI, KICP and Physics Department, Univ. of Chicago, Chicago, IL 60637*

Abstract

Electroweak baryogenesis in the minimal supersymmetric extension of the Standard Model may be realized within the light stop scenario, where the right-handed stop mass remains close to the top-quark mass to allow for a sufficiently strong first order electroweak phase transition. All other supersymmetric scalars are much heavier to comply with the present bounds on the Higgs mass and the electron and neutron electric dipole moments. Heavy third generation scalars render it necessary to resum large logarithm contributions to perform a trustable Higgs mass calculation. We have studied the one-loop RGE improved effective theory below the heavy scalar mass scale and obtained reliable values of the Higgs mass. Moreover, assuming a common mass \tilde{m} for all heavy scalar particles, and values of all gaugino masses and the Higgsino mass parameter about the weak scale, and imposing gauge coupling unification, a two-loop calculation yields values of the mass \tilde{m} in the interval between three TeV and six hundred TeV. Furthermore for a stop mass around the top quark mass, this translates into an upper bound on the Higgs mass of about 150 GeV. The Higgs mass bound becomes even stronger, of about 129 GeV, for the range of stop and gaugino masses consistent with electroweak baryogenesis. The collider phenomenology implications of this scenario are discussed in some detail.

1 INTRODUCTION

The minimal supersymmetric extension of the Standard Model (MSSM) has become the preferred candidate for the ultraviolet completion of the Standard Model (SM) beyond the TeV scale. The MSSM description may be extended up to a high (GUT or Planck) scale, and the search for supersymmetric particles is therefore one of the main experimental goals at the forthcoming Large Hadron Collider (LHC) at CERN. Among its main virtues, on top of solving the hierarchy problem of the Standard Model, the MSSM leads to a natural unification of the gauge couplings consistent with precision electroweak data and provides a natural candidate for the Dark Matter of the Universe (namely the lightest neutralino).

On the other hand electroweak baryogenesis [1] is a very elegant mechanism for generating the baryon asymmetry of the Universe that can be tested at present accelerator energies and, in particular, at the future LHC. It turns out that electroweak baryogenesis can not be realized within the Standard Model [2, 3], while it is not a generic feature of the MSSM for arbitrary values of its parameters [4, 5]. However, a particular region in the space of supersymmetric parameters was found in the MSSM, where electroweak baryogenesis has a chance of being successful [6], dubbed under the name of light stop scenario (LSS).

Since the generation of the BAU in the LSS is challenging other alternatives (where the right-handed stop is not singled out) have been explored in the literature. In particular in the context of split supersymmetry, and if one allows R_p -violating couplings, it was proven in Ref. [7] that superheavy squarks can produce enough baryon asymmetry when they decay out-of-equilibrium, while some splitting between left and right-handed mass squarks is required by the gluino cosmology. Moreover beyond the MSSM there are plenty of other possibilities. The simplest one is introducing singlets in the MSSM light spectrum (the so-called NMSSM [8] or nMSSM [9]), or even adding an extra Z' gauge boson [10], which easily triggers a strong first order phase transition.

Since the generation of the BAU in the MSSM has inherent uncertainties of order one, large variations in the final results appear due to the different approaches which have been considered in the literature [11]¹. According to these results, it looks possible to achieve the proper baryon asymmetry fulfilling all experimental bounds and in view of the forthcoming LHC running, it is worth refining the predictions of the LSS. In this paper we will then consider the effective theory of the LSS while in a companion paper [13] the phase transition will be analyzed in great detail using the results provided by the present analysis.

The light stop scenario of the MSSM is characterized by a light right-handed stop (with a mass near the top quark mass) while all other squarks and sleptons should be heavy enough in order to cope with present LEP bounds on the Higgs mass and to avoid large flavor, CP violation and electric dipole moment effects [14, 15]. On the other hand,

¹For instance, a possible contribution to the baryon asymmetry coming from light sbottoms and staus have been recently explored in Ref. [12].

supersymmetric fermions (Higgsinos and gauginos) are required to be at the electroweak (EW) scale (this fact can be technically natural as a consequence of some partly conserved R -symmetry) in order to trigger the required CP-violating currents needed for baryogenesis [11], as well as providing a Dark Matter candidate [16]. Moreover even if the LSS is consistent with a light CP-odd Higgs boson, a large splitting between the lightest CP-even Higgs and the CP-odd Higgs masses helps to avoid all phenomenological constraints, because it emulates the Standard Model Higgs sector at low energy (LE).

In practice we will consider all heavy scalars (sleptons, non-SM Higgs bosons and squarks, except for the right-handed stop) at a common scale \tilde{m} and study the LE Effective Theory (ET) below that scale. We will use the \overline{MS} renormalization scheme and resum the large logarithms which will appear in the calculation of various observables by using Renormalization Group Equations (RGE) techniques. In particular we will make use of the run-and-match technique [17] by which every particle decouples at its mass scale using the step-function approximation. The high-energy (HE) and LE theories, with different RGE in both regions, should match at the decoupling scale providing (finite) thresholds for the various couplings. In this way, considering a common decoupling scale is an approximation which amounts to neglect possible thresholds corresponding to the mass differences around \tilde{m} , and that should not affect our results in a significant way.

For very large values of \tilde{m} the model is a variant of Split Supersymmetry [18], where the right-handed stop is also (light) in the LE theory. Thus in the spirit of Split Supersymmetry every light particle is required by one particular experimental input: apart from the light Higgs, required by electroweak symmetry breaking, the light stop is required to trigger a strong enough first order phase transition while light charginos and neutralinos are required to generate enough baryon asymmetry and to become dark matter candidates. On the other hand gauge coupling unification, which works reasonably well in the MSSM, is an important issue. As we will see a two-loop analysis points towards values of \tilde{m} between ten and one hundred TeV for the case where all gauginos are at the electroweak scale, and around one order of magnitude larger for hierarchical gaugino masses as required by gaugino mass unification and by electroweak baryogenesis.

The outline of this paper is as follows. In Section 2 we present our LE effective theory below \tilde{m} as well as the matching conditions between the couplings of LE and HE theories, the threshold conditions for the different couplings and the β -functions in the LE Effective Theory. The technical details of the calculation of threshold conditions are presented in Appendix A and those about the RGE in Appendix B. In section 3 we present the numerical results based on the calculation of the previous section. In particular, the predictions of different parameters in the LE effective theory and the corresponding value of the Higgs mass. In Section 4 we consider the issue of gauge coupling unification. We show that the unification scale is $M_{GUT} = 1 \div 2 \times 10^{16}$ GeV while imposing the experimental value for the strong coupling leads to values of the heavy sfermion masses \tilde{m} in good agreement with the values of the parameters required to fulfill the electric dipole moment constraints in the EWBG scenario within the MSSM [14, 15, 16]. In Section 5 we present

some ideas for the experimental detection of \tilde{t}_R in our model, as well as the possibility of having a Dark Matter candidate. Finally in Section 6 we present our conclusions.

2 THE EFFECTIVE THEORY

The theory at an energy scale τ between the EW scale and \tilde{m} , at which supersymmetry is broken, contains all the SM particles and the Bino, Winos and Higgsinos, as well as the light stop. All other squarks and sleptons are heavy, with masses about \tilde{m} , and decouple from the low energy theory. The gluino, with a mass M_3 much below \tilde{m} , may be much heavier than the other gauginos and, in this case, when $\tau < M_3$ it will decouple too. Therefore the corresponding low energy effective Lagrangian is given by

$$\begin{aligned} \mathcal{L}_{eff} = & m^2 H^\dagger H - \frac{\lambda}{2} (H^\dagger H)^2 - h_t [\bar{q}_L \epsilon H^* t_R] + Y_t [\bar{H}_u \epsilon q_L \tilde{t}_R^*] \\ & - \frac{M_3}{2} \Theta_{\tilde{g}} \tilde{g}^a \tilde{g}^a - \frac{M_2}{2} \tilde{W}^A \tilde{W}^A - \frac{M_1}{2} \tilde{B} \tilde{B} - \mu \tilde{H}_u^T \epsilon \tilde{H}_d - M_U^2 |\tilde{t}_R|^2 \\ & - \sqrt{2} \Theta_{\tilde{g}} G \tilde{t}_R \tilde{g}^a \tilde{T}^a \tilde{t}_R + \sqrt{2} J \tilde{t}_R \tilde{B} \tilde{t}_R - \frac{1}{6} K |\tilde{t}_R|^2 |\tilde{t}_R|^2 - Q |\tilde{t}_R|^2 |H|^2 + h.c. \\ & + \frac{H^\dagger}{\sqrt{2}} (g_u \sigma^a \tilde{W}^a + g'_u \tilde{B}) \tilde{H}_u + \frac{H^T \epsilon}{\sqrt{2}} (-g_d \sigma^a \tilde{W}^a + g'_d \tilde{B}) \tilde{H}_d + h.c. , \end{aligned} \quad (2.1)$$

where the gluino decoupling is taken into account by the symbol $\Theta_{\tilde{g}}$ which is equal to 1 (0) for $\tau \geq M_3$ ($\tau < M_3$). For simplicity in (2.1) we do not write the kinetic terms explicitly and we approximate the Lagrangian by taking into account only interactions of the SM fields, charginos, neutralinos and the right-handed stop coming from renormalizable high energy terms proportional to the gauge couplings g', g, g_3 or the supersymmetric top Yukawa coupling λ_t without considering flavour mixing. Furthermore in (2.1) the field H is defined as the light projection of the MSSM Higgs bosons, given by $H_u \rightarrow \sin \beta H$, $H_{d,i} \rightarrow \cos \beta \epsilon_{ij} H_j^*$, with $\tan \beta \equiv \langle H_u^0 \rangle / \langle H_d^0 \rangle$.

At the energy scale \tilde{m} the effective Lagrangian (2.1) has to describe the physics of the HE theory, which implies that the following one-loop *matching conditions* have to be satisfied

$$Q(\tilde{m}) - \Delta Q = \left(\lambda_t^2(\tilde{m}) \sin^2 \beta + \frac{1}{3} g'^2(\tilde{m}) \cos 2\beta \right) \left(1 - \frac{1}{2} \Delta Z_Q \right) , \quad (2.2)$$

$$\lambda(\tilde{m}) - \Delta \lambda = \frac{g^2(\tilde{m}) + g'^2(\tilde{m})}{4} \cos^2 2\beta \left(1 - \frac{1}{2} \Delta Z_\lambda \right) , \quad (2.3)$$

$$K(\tilde{m}) - \Delta K = \left(g_3^2(\tilde{m}) + \frac{4}{3} g'^2(\tilde{m}) \right) \left(1 - \frac{1}{2} \Delta Z_K \right) , \quad (2.4)$$

$$G(\tilde{m}) - \Delta G = g_3(\tilde{m}) \left(1 - \frac{1}{2} \Delta Z_G \right) , \quad (2.5)$$

$$h_t(\tilde{m}) - \Delta h_t = \lambda_t(\tilde{m}) \sin \beta \left(1 - \frac{1}{2} \Delta Z_{h_t} \right) , \quad (2.6)$$

$$Y_t(\tilde{m}) - \Delta Y_t = \lambda_t(\tilde{m}) \left(1 - \frac{1}{2} \Delta Z_{Y_t} \right), \quad (2.7)$$

$$g_u(\tilde{m}) = g(\tilde{m}) \sin \beta, \quad g_d(\tilde{m}) = g(\tilde{m}) \cos \beta, \quad (2.8)$$

$$g'_u(\tilde{m}) = g'(\tilde{m}) \sin \beta, \quad g'_d(\tilde{m}) = g'(\tilde{m}) \cos \beta, \quad (2.9)$$

$$J(\tilde{m}) = \frac{2}{3} g'(\tilde{m}), \quad (2.10)$$

where the quantities ΔQ , $\Delta \lambda$, ΔK , ΔG , Δh_t , ΔY_t and ΔZ_i are the *threshold* functions. In particular ΔZ_i are the wave function thresholds coming from the matching of low and high energy propagators and the canonical normalization of ET kinetic terms while the others come directly from the matching of the low and high energy proper vertices (details of the calculation are given in Appendix A).

In this work we will consider for the threshold and β -functions the leading contributions and thus we will use the approximation of neglecting the one-loop corrections proportional to g' , g and the Yukawa couplings other than that of the top-quark (as well as the low energy couplings correlated to those). Following this criterion we consider no threshold in the matchings (2.8)-(2.10) since they do not appear at tree-level and would correspond to the one-loop corrections that we are neglecting.

The same analysis has to be redone when the renormalization scale τ becomes lower than M_3 and the gluino decouples. In this case the interaction term of (2.1) involving the coupling G disappears and the following matching conditions relate the values of the couplings before and after the gluino decoupling:

$$\begin{aligned} Q(M_3^-) &= Q(M_3^+)(1 - \Delta' Z_{\tilde{t}_R}), \\ K(M_3^-) &= K(M_3^+)(1 - 2\Delta' Z_{\tilde{t}_R}) + \Delta' K, \\ h_t(M_3^-) &= h_t(M_3^+)(1 - \Delta' Z_{t_R}/2), \\ Y_t(M_3^-) &= Y_t(M_3^+)(1 - \Delta' Z_{\tilde{t}_R}/2), \\ M_U^2(M_3^-) &= M_U^2(M_3^+)(1 - 2\Delta' Z_{\tilde{t}_R}) + \Delta' M_U^2, \end{aligned} \quad (2.11)$$

where $\Delta' Z_{\tilde{t}_R}$ ($\Delta' Z_{t_R}$) is the wave function threshold of the right stop (top) and $\Delta' K$ and $\Delta' M_U^2$ are the proper vertex threshold. The matching conditions of the couplings absent from (2.11) are trivial since they have no threshold discontinuity when the renormalization scale crosses M_3 . Readers interested in the explicit form of the thresholds of (2.2)-(2.11) can find them in Appendix A, Eqs. (A.7)-(A.13) and (A.19).

For energy scales between the top mass and \tilde{m} , at which all scalars apart from the right-handed stop and the Standard Higgs doublet are decoupled, one can compute the one-loop β -functions of the gauge constants ² in a straightforward way

$$(4\pi)^2 \beta_{g_i} = g_i^3 b_i \quad \text{with} \quad b = \left(\frac{143}{30}, -\frac{7}{6}, -\frac{41}{6} + 2\Theta_{\tilde{g}} \right),$$

²The two-loop beta functions will be given in Section 4 where the issue of gauge coupling unification is considered.

where we have used the GUT convention $g_1^2 = (5/3)g'^2$.

For the RGE of the other couplings we will only report their expressions and leave the calculation details to Appendix B. For the dimensionless couplings we obtain

$$\begin{aligned}
(4\pi)^2 \beta_{g_u} &= g_u \left(3h_t^2 + \frac{3}{2}Y_t^2 \right), \quad (4\pi)^2 \beta_{g_d} = 3 g_d h_t^2, \\
(4\pi)^2 \beta_{g'_u} &= g'_u \left(3h_t^2 + \frac{3}{2}Y_t^2 \right), \quad (4\pi)^2 \beta_{g'_d} = 3 g'_d h_t^2, \\
(4\pi)^2 \beta_J &= J \left(h_t^2 + 2Y_t^2 + \frac{12}{3} G^2 \Theta_{\tilde{g}} - 4g_3^2 \right), \\
(4\pi)^2 \beta_{Y_t} &= \frac{1}{2} Y_t \left(h_t^2 + 8Y_t^2 + \frac{16}{3} G^2 \Theta_{\tilde{g}} - 8g_3^2 \right), \\
(4\pi)^2 \beta_G &= \frac{1}{2} G \left(9G^2 + 2h_t^2 - 26g_3^2 + 4Y_t^2 \right), \\
(4\pi)^2 \beta_{h_t} &= h_t \left(\frac{9}{2} h_t^2 + \frac{1}{2} Y_t^2 + \frac{4}{3} G^2 \Theta_{\tilde{g}} - 8g_3^2 \right), \\
(4\pi)^2 \beta_\lambda &= 12\lambda^2 + 6Q^2 - 12h_t^4 + 12h_t^2 \lambda, \\
(4\pi)^2 \beta_Q &= -\frac{32}{3} G^2 h_t^2 \Theta_{\tilde{g}} - 4Y_t^2 h_t^2 + Q \left(K + 3\lambda + 4Q + 6h_t^2 + 4Y_t^2 + \frac{16}{3} G^2 \Theta_{\tilde{g}} - 8g_3^2 \right), \\
(4\pi)^2 \beta_K &= 12Q^2 + 13g_3^4 - \frac{88}{3} G^4 \Theta_{\tilde{g}} - 24Y_t^4 + K \left(\frac{14}{3} K + 8Y_t^2 + \frac{32}{3} G^2 \Theta_{\tilde{g}} - 16g_3^2 \right),
\end{aligned} \tag{2.12}$$

and for the dimensionful ones

$$\begin{aligned}
(4\pi)^2 \beta_\mu &= \frac{3}{2} \mu Y_t^2, \\
(4\pi)^2 \beta_{M_1} &= \mathcal{O}(g_1^2), \quad (4\pi)^2 \beta_{M_2} = \mathcal{O}(g_2^2), \\
(4\pi)^2 \beta_{M_3} &= M_3 (-18g_3^2 + G^2), \\
(4\pi)^2 \beta_m &= -6Q M_U^2 + 6m^2 h_t^2, \\
(4\pi)^2 \beta_{M_U^2} &= M_U^2 \left(\frac{8}{3} K + 4Y_t^2 + \frac{16}{3} G^2 - 8g_3^2 \right) - \frac{32}{3} M_3^2 G^2 \Theta_{\tilde{g}} - 4m^2 Q - 4Y_t^2 \mu^2,
\end{aligned} \tag{2.13}$$

where β_G and β_{M_3} make sense only for $\tau \geq M_3$.

3 NUMERICAL RESULTS ON THE HIGGS MASS

In this section we will apply the previous results to obtain in an appropriate way the values of the LE couplings and the Higgs mass at the EW scale for any large value of the cutoff scale \tilde{m} and for different values of the HE supersymmetric parameters.

3.1 RUNNING OF COUPLINGS

We need to know all the couplings of (2.1) at the EW scale that we identify here with the top-quark mass $m_t = 172.5 \pm 2.7$ GeV [19] (corresponding to $h_t(m_t) \simeq 0.95$). All

the mass parameters M_U^2, μ, M_3 are free inputs of the theory and thus we choose them directly at low energy by fixing $M_U^2(m_t), \mu(m_t), M_3(M_3)$. Moreover at the low scale also the SM couplings $g(\tilde{m}), g'(\tilde{m}), g_3(\tilde{m}), h_t(\tilde{m})$ and $m^2(m_t)$ are fixed experimentally³. On the contrary the non-SM couplings are defined by (2.2)-(2.10) at high energy as functions of the previous couplings, run up to the scale \tilde{m} , and the free quantities $\tilde{m}, \tan \beta$ and $A_t(\tilde{m})$. Therefore in order to get the non-SM couplings at the EW scale we have to solve a system of linear differential equations [the RGE (2.12)-(2.13)] with boundary condition in $\tau = m_t, M_3, \tilde{m}$. Equations must be solved numerically and iteratively because the conditions at the boundary \tilde{m} (2.2)-(2.10) depend in turn on the evolution of the parameters. The implicit resummation of the leading logarithms renders our estimation of the ET couplings reliable, even for large values of \tilde{m} . Using this procedure the values of the LE couplings at

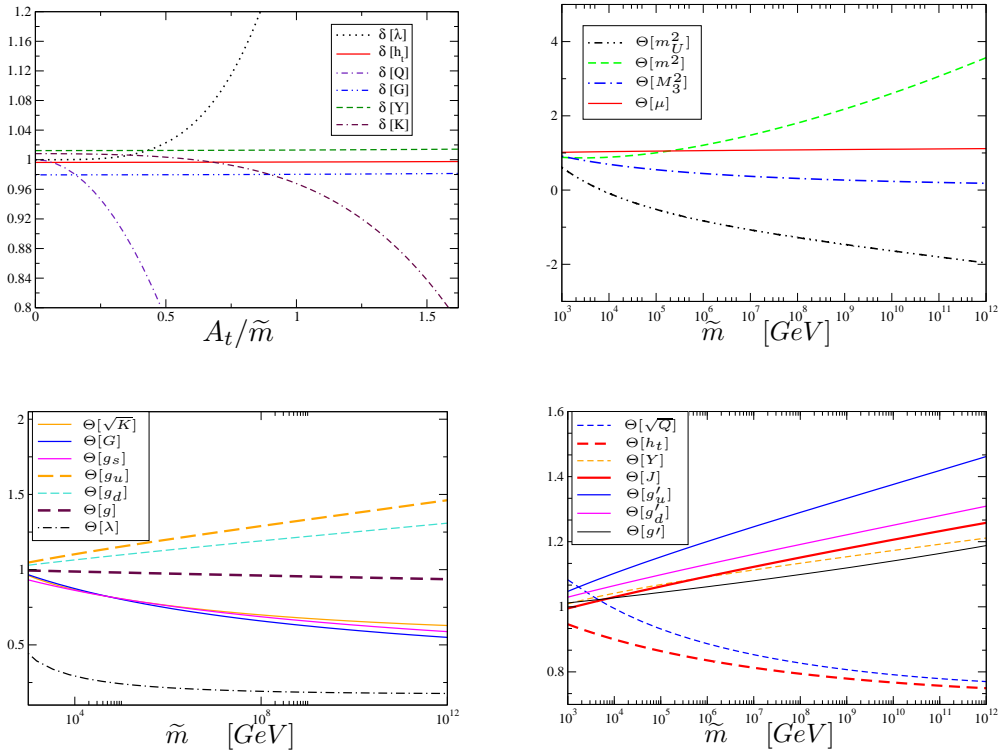


Figure 1: Upper-left panel: We plot for every coupling the ratio δ of its value at the decoupling scale \tilde{m} over its value without any threshold contribution, as a function of A_t/\tilde{m} for $\tilde{m} = 100$ TeV. Upper-right and lower panels: the ratio Θ between the couplings at $\tau = m_t$ and their starting value at $\tau = \tilde{m}$ (for the coupling M_3 and G the lower τ value is $\tau = M_3$) is plotted as function of \tilde{m} , for $A_t = 0.6 \tilde{m}$. In all plots $\tan \beta = 2$, $M_U = 200$ GeV, $M_3 = 500$ GeV and $\mu = 100$ GeV have been fixed.

³The parameter $m^2(m_t)$ is fixed by the condition that the minimum of the SM-like Higgs one-loop potential be $v = 246.22$ GeV at the scale m_t .

the EW scale will basically depend on two different factors: the matching conditions and the running evolution. Focusing on the former in the upper-left panel of Fig. 1 we analyze the thresholds relevance by plotting for every coupling the ratio (defined as δ in the plot) of its value over the one without the threshold contribution, both evaluated at the scale \tilde{m} , as functions of A_t/\tilde{m} for $\tan\beta = 2$, $M_U = 200$ GeV, $M_3 = 500$ GeV, $\mu = 100$ GeV, and $\tilde{m} = 100$ TeV. It is remarkable that the threshold contributions to the couplings λ , Q and K can easily reach a value $\sim 10\%$ and beyond, unlike the h_t, Y, G -thresholds which are almost A_t -independent and remain below $\sim 2\%$ ⁴. For this reason it is sensible to neglect the threshold effects of h_t, Y, G , since their contributions are within the uncertainty of our approximations.

The relevance of the running is also exhibited in Fig. 1 where the ratios $\rho(\tilde{m})/\rho(X) \equiv \Theta[\rho]$ for all couplings ρ are plotted as functions of \tilde{m} (where $X = M_3$ for $\rho = M_3, G$ and $X = m_t$ for the rest of couplings) for $A_t = 0.6\tilde{m}$ and keeping the rest of parameters fixed as in the upper-left plot. In particular in the upper-right panel we plot masses and in the lower panels all dimensionless couplings. For example we can compare from the lower-right figure how the couplings h_t and Y evolve differently, even if we had neglected their different threshold effects.

3.2 THE HIGGS MASS

Once we have computed the values of the couplings in (2.1) it is straightforward to obtain the Higgs effective potential in which the leading logarithms are resummed. Since this potential is strongly dependent on the renormalization scale we need to consider the one-loop part of the effective potential calculated in the LE theory. We are adding to the SM fields only the contribution from \tilde{t}_R since the contribution from charginos and neutralinos (which is numerically small) would spoil the scale invariance of the effective potential in our approximation where we are neglecting electroweak gauge couplings in the LE β -functions. The one-loop contributions to the effective potential then read as

$$V_{1-loop}(\phi_c) = \frac{6}{64\pi^2} \sum_i n_i m_i^4(\phi_c) \left(\ln \frac{m_i^2(\phi_c)}{\mu^2} - C_i \right) \quad \text{with } i = W, Z, h, \chi, \tilde{t}_R, t \quad (3.1)$$

where $C_W = C_Z = 5/6$, $C_h = C_\chi = C_{\tilde{t}_R} = C_t = 3/2$ and $n_W = n_{\tilde{t}_R} = 6$, $n_Z = 3$, $n_h = 1$, $n_\chi = 3$, $n_t = -12$ and the masses are

$$\begin{aligned} m_W^2 &= \frac{g^2}{4} \phi_c^2, & m_Z^2 &= \frac{g^2 + g'^2}{4} \phi_c^2, \\ m_h^2 &= \frac{\lambda}{2} (3\phi_c^2 - v^2), & m_\chi^2 &= \frac{\lambda}{2} (\phi_c^2 - v^2), \\ m_{\tilde{t}_R}^2 &= M_U^2 + \frac{Q}{2} \phi_c^2, & m_t^2 &= \frac{h_t^2}{2} \phi_c^2, \end{aligned} \quad (3.2)$$

⁴It has been checked that this estimate holds also for other values of \tilde{m} .

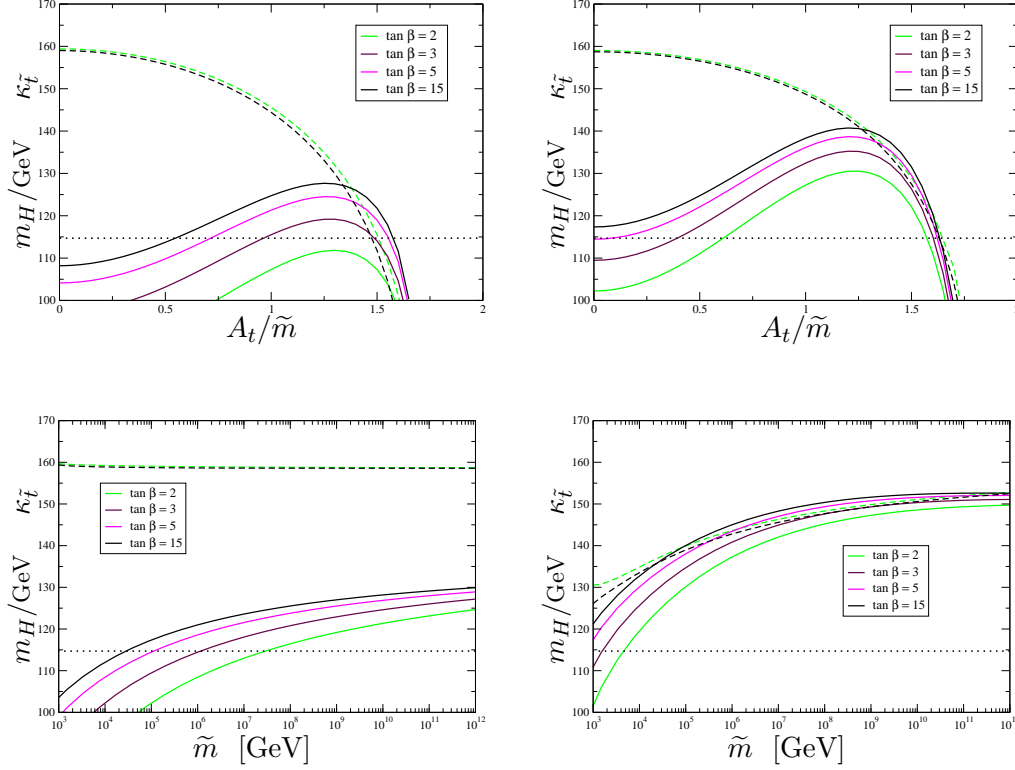


Figure 2: m_H/GeV (solid lines) and $\kappa_{\tilde{t}}$ (dashed curves) predicted for the case $M_U = 200$ GeV, $\mu = 100$ GeV and $M_3 = 500$ GeV for several values of $\tan\beta$. In the upper-left (upper-right) panel $\tilde{m} = 3$ (100) TeV has been fixed and in the lower-left (lower-right) panel $A_t = 0(1.3)\tilde{m}$. The experimental lower bound on the Higgs mass is marked by a dotted straight line.

with the renormalization scale conventionally chosen to be m_t . Notice that by this renormalization scale choice and thanks to the use of the LE theory the logarithms of (3.1) are always small. Moreover the addition of the one-loop contribution (3.1) eliminates the scale dependence of the potential proportional to strong-like or Yukawa-like couplings up to the one-loop order.

The second derivative of the potential at the EW minimum provides the Higgs mass within the one-loop renormalization group improved effective theory. The numerical result is shown in Fig. 2 where we plot the Higgs mass m_H (solid line). We also introduce the parameter $\kappa_{\tilde{t}} \equiv 10\sqrt{m_{\tilde{t}_R}}/\text{GeV}$ (dashed line) which parameterizes the lightest stop mass. The parameter $\kappa_{\tilde{t}}$ has the advantage of being related in a simple way to the stop mass, and since it acquires values similar to the Higgs mass (in GeV units), it may be represented together with it on a linear scale. Observe that $\kappa_{\tilde{t}} = 100$ is equivalent to $m_{\tilde{t}_R} = 100$ GeV and $m_{\tilde{t}_R} < m_t$ corresponds to $\kappa_{\tilde{t}} \lesssim 130$. Values of $\kappa_{\tilde{t}} \lesssim 100$ are therefore excluded by LEP searches. We plot both variables as functions of A_t/\tilde{m} [upper panels: on the left (right)

panel $\tilde{m} = 3$ (100) TeV] and \tilde{m} [lower panels: on the left (right) panel $A_t = 0$ ($1.3 \tilde{m}$)] for several values of $\tan \beta$.

For m_H and $\kappa_{\tilde{t}}$ the different values of $\tan \beta$ are encoded by different colours (level of line darkness) presented in the legend. Since a change of $\tan \beta$ does not appreciably modify $\kappa_{\tilde{t}}$ we mark only the extremal curves corresponding to $\tan \beta = 15$ and $\tan \beta = 2$. In all the plots we have fixed $M_U = 200$ GeV, $\mu = 100$ GeV and $M_3 = 500$ GeV.

Some comments on the different masses can be easily drawn from Fig. 2. We notice that because of the experimental bound on the Higgs mass, $m_H > 114.7$ GeV [19] (dotted straight line in Fig. 2) the model with $\tilde{m} \sim 1$ TeV requires $\tan \beta > 3$ and in general the smaller $\tan \beta$ is the closer to $1.3 \tilde{m}$ the trilinear coupling A_t has to be since the Higgs mass has a maximum there. This requirement is relaxed if \tilde{m} is increased, but scales as large as $\tilde{m} \simeq 10^7$ TeV are necessary to overcome the Higgs mass bound for any $\tan \beta \gtrsim 2$ independently of A_t . On the contrary if we allow $A_t \simeq 1.3 \tilde{m}$ the model is experimentally safe for $\tan \beta \geq 2$ already at $\tilde{m} = 5$ TeV. On the other hand if we require the right-handed stop to be lighter than the top quark ($\kappa \lesssim 130$) with $M_U^2 \sim (200 \text{ GeV})^2$ a large A_t is needed. Another way to maintain the stop lighter than the top quark is by decreasing M_U^2 , which lowers the stop mass. For $M_U^2 \lesssim (100 \text{ GeV})^2$ the maxima of the Higgs mass curves are excluded by the LEP bound on the stop mass. Consequently the bounds on $\tan \beta$, A_t and \tilde{m} become even stronger in this case.

The latter result applies, in particular, for the conditions which are favorable to electroweak baryogenesis (EWBG) where $M_U^2 < 0$ is needed. As an example, in Fig. 3 we choose the same parameters as in Fig. 2 but with a right-handed stop mass parameter $M_U^2 = -(100 \text{ GeV})^2$ and $\tilde{m} = 100$ (1000) TeV in the upper-left (right) plot. We can see from the right-panel of Fig. 3 that there exists the upper bound $A_t \lesssim 0.6 \tilde{m}$ coming from the experimental bounds on the stop mass. Notice that, independently of the experimental bounds, larger values of A_t/\tilde{m} would lead to an instability of the electroweak minimum. Moreover values of $A_t/\tilde{m} \lesssim 0.5$ are also required in order to obtain a strong enough electroweak phase transition [6]. On the other hand the rough estimate $\tan \beta \lesssim 10$ [14, 16], coming from the requirement of generation of the observed baryon asymmetry of the Universe, pushes the parameter \tilde{m} towards values $\tilde{m} \gg 1$ TeV which justifies a posteriori the study of the effective theory with resummed logarithms. A detailed analysis of electroweak baryogenesis in the present model will be thoroughly analyzed in Ref. [13]. Let us stress that values of $\tilde{m} \gg 1$ TeV are consistent with those necessary in order to suppress the one-loop contributions to the electric dipole moment of the electron and the neutron in the light stop scenario [15].

Finally let us observe that all previous comments, which apply for a gluino mass of 500 GeV, can also be extended to other values of the gluino masses. In particular we have checked that for $M_3 \simeq 1$ TeV the Higgs mass only decreases by a few percent with respect to the case of gluino masses at the EW scale.

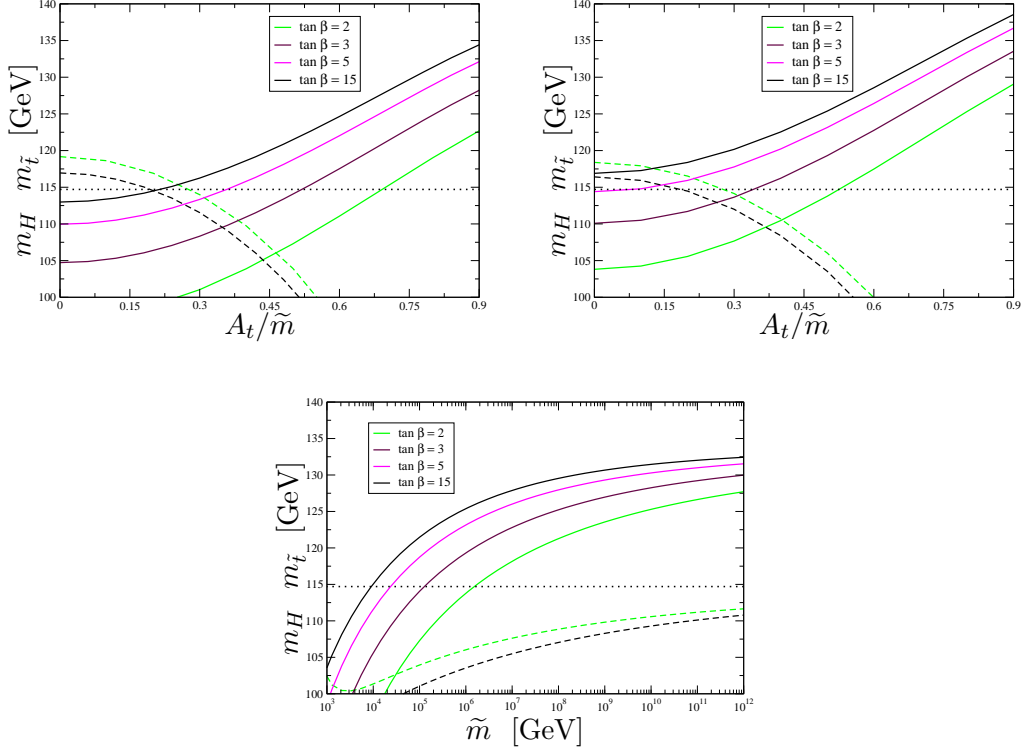


Figure 3: Plots similar to those in upper panels of Fig. 2, but with a different value of M_U [$M_U^2 = -(100 \text{ GeV})^2$] and of \tilde{m} ($\tilde{m} = 100 \text{ TeV}$ in the left panel and $\tilde{m} = 1000 \text{ TeV}$ in the right one). The lower plot is done with $A_t/\tilde{m} = 0.5$.

4 GAUGE COUPLING UNIFICATION

In this section we will consider the issue of gauge coupling unification in the theory where below the scale \tilde{m} there is the ET which has been considered in Section 2 and beyond \tilde{m} the MSSM. In the extreme case where \tilde{m} is at the EW scale, the condition of gauge coupling unification yields low energy values for the strong gauge coupling α_3 consistent with those obtained in low energy MSSM scenarios. The MSSM prediction, however, depends strongly on the possible threshold corrections to the gauge couplings at the GUT scale, as well as on the additional threshold corrections induced by the weak scale supersymmetric particles. Ignoring high-energy threshold corrections, one obtains a range of values $\alpha_3(M_Z) = 0.120$ – 0.135 , with the exact value depending on the precise MSSM spectrum. This range of values is compatible with experimental data, but with some tension towards a predicted high value. When \tilde{m} is increased the predicted value of $\alpha_3(M_Z)$ coming from the requirement of gauge coupling unification moves towards lower values. Therefore for a given low energy spectrum one can find agreement with the experimental values for a certain range of values of \tilde{m} . In this sense it is possible to make a grand unification “prediction” for the parameter

\tilde{m} . High energy threshold corrections would lead to an uncertainty on this range of \tilde{m} values. In this section, we will quantify these issues after considering the two-loop RG evolution of the gauge couplings.

The two-loop renormalization-group equation for the gauge couplings are [20]

$$(4\pi)^2 \frac{d}{dt} g_i = g_i^3 b_i + \frac{g_i^3}{(4\pi)^2} \left[\sum_{j=1}^3 B_{ij} g_j^2 - d_i^u h_t^2 - d_i^W (\tilde{g}_u^2 + \tilde{g}_d^2) - d_i^B (\tilde{g}_u'^2 + \tilde{g}_d'^2) - d_i^G G^2 - d_i^J J^2 \right] \quad (4.1)$$

where $t = \ln \tau$, τ is the renormalization scale and we use the convention $g_1^2 = (5/3)g'^2$. Eq. (4.1) is scheme-independent up to the two-loop order.

In the effective theory below \tilde{m} , the β -function coefficients are

$$b = \left(\frac{143}{30}, -\frac{7}{6}, -\frac{41}{6} + 2\Theta_{\tilde{g}} \right), \quad B = \begin{pmatrix} \frac{376}{75} & \frac{18}{5} & \frac{196}{15} \\ \frac{6}{5} & \frac{106}{3} & 12 \\ \frac{49}{30} & \frac{9}{2} & -\frac{67}{3} + 48\Theta_{\tilde{g}} \end{pmatrix}, \quad (4.2)$$

$$d^u = \left(\frac{17}{10}, \frac{3}{2}, 2 \right), \quad d^G = \left(\frac{32}{10}, 0, \frac{13}{2} \right) \Theta_{\tilde{g}}, \quad d^J = \left(\frac{18}{5}, 0, 1 \right), \quad (4.3)$$

$$d^W = \left(\frac{9}{20}, \frac{11}{4}, 0 \right), \quad d^B = \left(\frac{3}{20}, \frac{1}{4}, 0 \right), \quad (4.4)$$

while above \tilde{m} one has the MSSM result [replacing in (4.1) the SM Yukawa h_t by the MSSM one λ_t related to the former by (2.6)] [21]

$$b = \left(\frac{33}{5}, 1, -3 \right), \quad B = \begin{pmatrix} \frac{199}{25} & \frac{27}{5} & \frac{88}{5} \\ \frac{9}{5} & 25 & 24 \\ \frac{11}{5} & 9 & 14 \end{pmatrix}, \quad (4.5)$$

$$d^u = \left(\frac{26}{5}, 6, 4 \right), \quad d^G = d^J = d^W = d^B = 0. \quad (4.6)$$

Finally the one-loop RGE of the Yukawa-like and gauge-like couplings are given in Eq. (2.12), while for the supersymmetric Yukawa coupling [21]

$$(4\pi)^2 \frac{d\lambda_t}{dt} = \lambda_t \left[-\frac{13}{15} g_1^2 - 3g_2^2 - \frac{16}{3} g_3^2 + 6\lambda_t^2 \right]. \quad (4.7)$$

We will consider the following experimental inputs [19]

$$\sin^2 \theta_{\overline{MS}}(M_Z) = 0.2312 \pm 0.0002, \quad (4.8)$$

$$\alpha_{EM}^{-1}(M_Z) = 127.906 \pm 0.019, \quad (4.9)$$

$$\alpha_3(M_Z) = 0.1176 \pm 0.0020, \quad (4.10)$$

and by imposing unification of $\alpha_1(M_{GUT}) = \alpha_2(M_{GUT})$ we obtain a prediction for $\alpha_3(M_Z)$ as it is shown in the left panel of Fig. 4. The solid black line in the left panel of Fig. 4

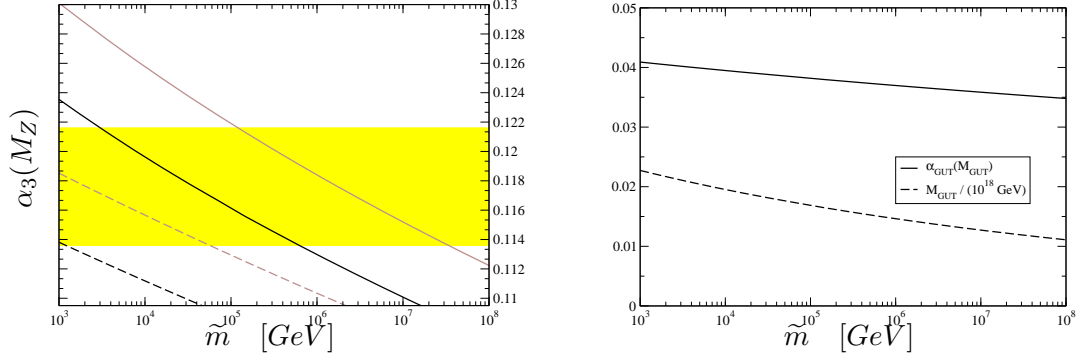


Figure 4: Predicted values of $\alpha_3(M_Z)$ [left panel: black lines are for all gauginos at the EW scale and grey lines for all gauginos at the EW scale except for the gluino with a mass $M_3 = 500$ GeV] by means of the two-loop (solid line) and one-loop (dashed-line) RG evolution, and the resulting two-loop predictions for M_{GUT} and α_{GUT} [right panel] as functions of \tilde{m} from the unification condition. The (yellow) band shows the experimental value of $\alpha_3(M_Z)$ within 2σ .

represents the two-loop result for values of all gaugino masses about the weak scale, while the dashed black line represents the one-loop result. The grey lines are corresponding plots for a gluino mass $M_3 = 500$ GeV, which roughly follows the gaugino mass unification relation $M_3/M_2 \simeq 3$. In the figure the experimental value of $\alpha_3(M_Z)$ within 2σ is marked by a (yellow) band. For our two choices of M_3 the gluino decoupling almost does not modify the curves of M_{GUT} and α_{GUT} as function of \tilde{m} and for this reason in the right panel we do not differentiate between both cases. Using the experimental value for the strong coupling one can get for the case where all gauginos are at the EW scale the 1σ prediction for \tilde{m} as

$$\tilde{m} \simeq 10^{1.6 \pm 0.6} \text{ TeV} . \quad (4.11)$$

If one considers instead the standard unification relation between the gaugino masses the predicted values of $\alpha_3(M_Z)$ would be shifted to larger values, $\Delta\alpha_3(M_Z) \simeq 0.005$ and the resulting values of \tilde{m} will be shifted up to

$$\tilde{m} \simeq 10^{3.3 \pm 0.6} \text{ TeV} . \quad (4.12)$$

For these two ranges of \tilde{m} altogether the unification scale M_{GUT} turns out to be all in all $1 \div 2 \times 10^{16}$ GeV, where the smaller value is referred to the largest available \tilde{m} value.

The numerical results may be analytically understood by considering the modifications of the two-loop predictions for $\alpha_3(M_Z)$ by one-loop threshold corrections induced by the supersymmetric particles,

$$\alpha_3(M_Z) = \alpha_3(M_Z)|_{\text{MSSM}} - \alpha_3^2(M_Z)|_{\text{MSSM}} \frac{19}{28\pi} \ln \left(\frac{T_{\text{MSSM}}}{M_Z} \right) , \quad (4.13)$$

where [22]

$$T_{MSSM} = |\mu| \left(\frac{M_2}{M_3} \right)^{28/19} \left(\frac{M_2}{|\mu|} \right)^{4/19} \left(\frac{\tilde{m}}{m_{\tilde{t}}} \right)^{5/19} \left(\frac{\tilde{m}}{|\mu|} \right)^{3/19}. \quad (4.14)$$

In the above $\alpha_3(M_Z)|_{\text{MSSM}} \simeq 0.127$ would be the value that would be obtained if all supersymmetric particles would have masses equal to M_Z . The second-to-last and last terms in Eq. (4.14) represent the effects of separating the stop mass with respect to the other sfermion masses and of increasing the non-SM Higgs doublet mass, respectively. In particular for the case in which all gaugino masses, $|\mu|$ and the light stop are of the order of the weak scale one can reproduce the 1σ prediction for \tilde{m} as given in Eq. (4.11), while in the case of standard unification relation of gaugino masses Eq. (4.12) is recovered if equal values of $|\mu|$ and M_2 of order of the weak scale are assumed. These low energy supersymmetric threshold effects may be compensated by thresholds at the GUT scale, which are strongly model dependent, but are naturally of the same order as the low energy supersymmetric thresholds (see, for instance Ref. [23]). Therefore for hierarchical gaugino masses, as the ones required by electroweak baryogenesis, the natural values of \tilde{m} necessary to achieve unification and consistent at 95 % C.L. with present experimental values of $\alpha_3(M_Z)$ are about 100 TeV. Somewhat lower values of \tilde{m} of the order of a few tens of TeV may be obtained by pushing $|\mu|$ to larger values.

The values of \tilde{m} consistent at 95 % C.L. with unification of couplings (for light gluinos $3 \text{ TeV} < \tilde{m} < 600 \text{ TeV}$ and for standard gaugino unification $100 \text{ TeV} < \tilde{m} < 3 \times 10^4 \text{ TeV}$) have an impact on the Higgs mass predictions. From Fig. 2, we can see that values of \tilde{m} larger than a few TeV lead to consistency with the LEP Higgs mass constraints for a large range of values of $\tan \beta$ when A_t/\tilde{m} is conveniently chosen. For the (positive) value of M_U^2 used in Fig. 2, $M_U^2 = (200 \text{ GeV})^2$, values of \tilde{m} of the order of 600 TeV ($3 \times 10^4 \text{ TeV}$) lead to maximum values of the Higgs mass around 144 (150) GeV. On the other hand, as shown in Fig. 3, for negative values of M_U^2 and $A_t \lesssim 0.5 \tilde{m}$, as required by electroweak baryogenesis, the values $\tilde{m} \simeq 600 \text{ TeV}$ ($3 \times 10^4 \text{ TeV}$) lead to maximum values of the Higgs boson mass around 125 (129) GeV.

5 MODEL COSMOLOGY AND COLLIDER PHENOMENOLOGY

The cosmology and collider phenomenology of the light stop scenario has been the subject of study of different articles. For masses below 135 GeV, as preferred by the electroweak baryogenesis scenario, the light stop mass will be in general smaller than the sum of the W mass, the b -quark mass and the lightest neutralino mass, and therefore its three body decay channels will be suppressed. Under these conditions, the main stop decay channel may be a loop-induced two body decay channel into a charm quark and the lightest neutralino. Searches for such a light stop at LEP put a bound on its mass of about 100 GeV [24].

Current searches at the Tevatron collider for a stop decaying into charm jets and neutralinos lead to a final state of two jets and missing energy. The jets should be sufficiently

energetic for the Tevatron to be able to trigger on those events, what in practice demands mass differences between the stops and the neutralinos of about 30 GeV or larger [25, 26]. Therefore the Tevatron collider cannot set any constraints on direct production of stops for mass differences smaller than 30 GeV. Searches for light stops in direct pair production of these particles, will be equally difficult at the LHC.

Small mass differences between the stop and the neutralino define a particularly interesting region of parameters since they are helpful in providing the proper dark matter density in scenarios with heavy fermions. Indeed, for mass differences of about 20 GeV, the co-annihilation between the stop and the lightest neutralino leads to a neutralino dark matter density consistent with experimental observations [16].

Searches for light stops at the LHC may proceed through additional production channels. For instance, the light stops may be produced from the decay of heavy gluinos. Assuming that the right-handed stops are the only squarks with masses below the gluino mass, as happens in the light stop scenario discussed in this article, the gluinos being Majorana particles may decay into a stop and an anti-top or into an anti-stop and a top-quark. One can then consider the decay of a pair of gluinos into two equal sign top-quarks and two stops (two charm jets and missing energy). It has been shown [27] that under these conditions, the light stops may be found even for small mass differences, of about 5 GeV, provided the heavy gluinos are lighter than about 900 GeV.

One would be interested in finding a method of stop detection that would be independent of the exact masses of other sparticles and which would work for small mass differences. A possibility is to analyze the possible production of light stops in association with a photon or a gluon (jet). The photon signatures are particularly clean, and for small mass differences they may be used as a complementary channel for the search for light stops at hadron colliders leading to a final state of two photons, soft jets and missing energy. Although not as clean as the photon signatures, due to larger rates, the jet plus missing energy signature may allow a further extension of the LHC reach for light stops. An analysis in this direction is in progress [28].

6 CONCLUSIONS

In this article we analyzed the light stop scenario in which all squarks and sleptons, apart from a mainly right-handed stop, are significant heavier than the weak scale. The large values of the scalars imply that the low energy effective theory predictions may only be evaluated in a precise way by resummation of the large leading logarithms associated with the decoupling of the heavy scalars. Since supersymmetry is broken at scales below the heavy scalar mass \tilde{m} , the Yukawa couplings associated with gauginos and Higgsinos must be computed, starting with their boundary values given by the gauge and supersymmetric Yukawa couplings respectively. Similarly the quartic couplings of the Higgs boson and the light top-squark may be computed through their RG evolution to lower energies.

We have applied the low energy effective theory to obtain a reliable computation of the

lightest CP-even Higgs boson mass for large values of \tilde{m} . In the extreme case where \tilde{m} is close to the EW scale, logarithm resummation is unnecessary and we have checked that our calculation of the SM-like Higgs is consistent with earlier calculations in the literature [30]. Since the quartic coupling is bounded by its relation with the weak gauge couplings plus finite threshold corrections at high energies, the Higgs mass remains bounded to small values, smaller than about 133 GeV for negative values of $M_U^2 \simeq -(100 \text{ GeV})^2$ and $A_t \lesssim 0.5 \tilde{m}$ even for large values of \tilde{m} . This has important implications for the realization of the electroweak baryogenesis scenario. In a general light stop scenario with no EWBG mechanism built in, this bound on the Higgs mass may be relaxed for positive values of M_U^2 , for which the trilinear mass parameter A_t may be pushed to larger values, leading to masses that may be as large as 152 GeV for large values of \tilde{m} .

We have also analyzed the issue of unification of gauge couplings. We have shown that the corrections induced by the heavy spectrum are helpful in rendering the measured values of the gauge couplings consistent with the unification conditions even for relatively large values of \tilde{m} . For instance considering universal values of the gaugino masses at low energies and values of $|\mu|$ of about 100 GeV, one obtains that appropriate unification is achieved for values of $\tilde{m} \simeq 10^{1.6 \pm 0.6} \text{ TeV}$. A similar result is obtained for the standard unification relation between the gaugino masses, for a Higgsino mass parameter of about 1 TeV. If $|\mu|$ takes values close to 100 GeV, instead, the value of \tilde{m} consistent with the unification of couplings is pushed up to $\tilde{m} \simeq 10^{3.3 \pm 0.6} \text{ TeV}$. This ranges of masses have implications on the predicted Higgs mass. For positive values for $M_U^2 \simeq (200 \text{ GeV})^2$, the ranges of values of \tilde{m} compatible at 95 % C.L. with gauge coupling unification lead to an upper bound on the Higgs mass of about 150 GeV. For negative values of M_U^2 and $A_t \lesssim 0.5 \tilde{m}$, as the ones required for baryogenesis, the upper bound becomes even stronger, of about 129 GeV.

The resulting phenomenology of the light stop scenario was also discussed in some detail. If a light Higgs, with mass $m_h \lesssim 133 \text{ GeV}$ is found, the next step to confirm the EWBG scenario within the MSSM would be the discovery of a light stop, with a mass below the top quark mass. Light stop searches at the Tevatron may lead to an experimental confirmation of this scenario, but may not be successful if the mass difference between the stop and the neutralino is smaller than about 30 GeV. Unfortunately, these small mass differences may be the ones required to obtain the proper dark matter relic density by means of coannihilation between the stop and the lightest neutralino. Searches at the LHC may be able to test the coannihilation region in case the gluino is lighter than about 900 GeV. For heavier gluino masses alternative methods of detection at the LHC via the production of light stops in association with photons or jets, are currently being studied and seem to be promising.

ACKNOWLEDGMENTS

We would like to thank C. Balazs, A. Freitas, T. Konstandin, D. Morrissey and A. Menon for useful discussions and interesting observations. Work supported in part by the European Commission under the European Union through the Marie Curie Research and Training Networks “Quest for Unification” (MRTN-CT-2004-503369) and “UniverseNet” (MR-TN-CT-2006-035863). Work at ANL is supported in part by US DOE, Division of HEP, Contract DE-AC-02-06CH11357 and Fermilab is operated by Fermi Research Alliance, LLC under Contract No. DE-AC02-07CH11359 with the United States Department of Energy. The work of M.Q. was partly supported by CICYT, Spain, under contract FPA 2005-02211.

APPENDIX

A THRESHOLDS

In this appendix we will give some details about the calculation of the different thresholds which appear in Section 2. At the renormalization scale \tilde{m} the ET (2.1) has to describe the same physics as its corresponding HE theory, the MSSM. Here we will match both theories at one-loop in the Landau gauge using the step-function approximation. Graphically the matching is presented in Figs. 5-11.

Since the matching has to be performed order by order in perturbation theory, we will start by considering the effective coupling Q , which is the only one having not trivial matching at tree-level (see Fig. 5). This matching can be easily solved by neglecting heavy field kinetic-terms and solving for their equation of motion. The result is given in (A.7).

At one-loop we cannot follow the same procedure because in dimensional regularization no kinetic-term can be neglected inside the loop. In such a case we can compute the diagrams in the LE and HE theories and, after using the tree-level matching conditions, impose the equivalence of the two results⁵. We will follow this diagrammatic approach only for the h_t , Y_t , G proper vertex matching, Figs. 6-8, and the wave function contribution furnished by each external leg (as an example we draw the case of \tilde{t}_R and t_R in Figs. 9 and 10). In fact in these cases identifying the threshold sources is straightforward. The corresponding HE diagrams are shown in Figs. 6-10. The resulting proper vertex thresholds are given in (A.8)-(A.10) and the wave function ones in (A.13). Finally for the proper vertex threshold $\Delta\lambda$ (ΔK) it is easier to match the one-loop Higgs (stop) LE and HE effective potentials, instead of performing the matching diagrammatically (see Fig. 11)⁶.

Let us start to explicitly analyze the case of $\Delta\lambda$ for which we have to impose the equivalence of the terms proportional to ϕ_c^4 after the expansion of the HE and LE effective

⁵Clearly, this operation is well defined only after fixing the subtraction scheme, in our case the \overline{MS} .

⁶In the Q matching condition we do not consider the one-loop proper vertex threshold since the tree-level one dominates.

potentials

$$\Lambda - \frac{m^2}{2}\phi_c^2 + \frac{\lambda}{8}\phi_c^4 + V_{LE}^h(\phi_c) = \Lambda' - \frac{m'^2}{2}\phi_c^2 + \frac{(g^2 + g'^2)}{32}\phi_c^4 \cos^2 2\beta + V_{HE}^h(\phi_c) + \mathcal{O}(\phi_c^5) \quad (\text{A.1})$$

where m^2 and Λ are equal to m'^2 and Λ' up to threshold effects coming from the difference between the one-loop contributions $V_{HE}^h(\phi_c)$ and $V_{LE}^h(\phi_c)$

$$\begin{aligned} & V_{HE}^h(\phi_c) - V_{LE}^h(\phi_c) \\ &= \frac{6}{64\pi^2} \sum_{r=\tilde{t}_1, \tilde{t}_2} m_r^4 \left(\ln \frac{m_r^2}{\tau^2} - \frac{3}{2} \right) - \frac{6}{64\pi^2} m_{\tilde{t}_R}^4 \left(\ln \frac{m_{\tilde{t}_R}^2}{\tau^2} - \frac{3}{2} \right), \end{aligned} \quad (\text{A.2})$$

where the renormalization scale is fixed to $\tau = \tilde{m}$, $m_{\tilde{t}_R}$ is explicit in (3.2) and \tilde{t}_1, \tilde{t}_2 are the eigenvalues of

$$\begin{pmatrix} \tilde{m}^2 + \lambda_t^2(\phi_c^2/2) \sin^2 \beta & -\lambda_t \tilde{A}_t(\phi_c/\sqrt{2}) \sin \beta \\ -\lambda_t \tilde{A}_t(\phi_c/\sqrt{2}) \sin \beta & M_U^2 + \lambda_t^2(\phi_c^2/2) \sin^2 \beta \end{pmatrix}, \quad (\text{A.3})$$

with $\tilde{A}_t = A_t - \mu/\tan \beta$. The threshold $\Delta\lambda$ can be derived extracting the coefficient of the term $\phi_c^4/8$ from the right-hand side of (A.2). Finally remembering that $\tilde{m}^2 \gg M_U^2$, we obtain the relation (A.11).

Following the same idea we can also obtain ΔK . We give a constant background s_c to the real third colour component of \tilde{t}_R , *i.e.* $\langle \tilde{t}_{R3} \rangle = s_c/\sqrt{2}$, which breaks the $SU(3)_c$ and $U(1)_Y$ symmetries, and we impose the equivalence of its one-loop effective potential in the LE and HE theory at the scale \tilde{m}

$$\Lambda + \frac{M_U^2}{2}s_c^2 + \frac{K}{24}s_c^4 + V_{LE}^{\tilde{t}_R}(s_c) = \Lambda' + \frac{M_U'^2}{2}s_c^2 + \frac{g_3^2}{24}s_c^4 + V_{HE}^{\tilde{t}_R}(s_c) + \mathcal{O}(s_c^5), \quad (\text{A.4})$$

where

$$V_{HE}^{\tilde{t}_R} - V_{LE}^{\tilde{t}_R} = \frac{4}{64\pi^2} \sum_{r=1}^5 m_r^4 \left(\log \frac{m_r^2}{\tau^2} - \frac{3}{2} \right) - \frac{4}{64\pi^2} \nu_H^4 \left(\log \frac{\nu_H^2}{\tau^2} - \frac{3}{2} \right), \quad (\text{A.5})$$

with $\tau = \tilde{m}$ and $\nu_H^2 = \lambda_t^2 \sin^2 \beta (1 - \frac{\tilde{A}_t^2}{\tilde{m}^2}) \frac{s_c^2}{2}$. Moreover for $r = 1, 2, 3$ the masses m_r^2 are the eigenvalues of the squared mass matrix of \tilde{q}_3 , H and H_h (the heavy projection of the Higgses: $H_u^\dagger \rightarrow \sin \beta H_h^t \epsilon$ and $H_d \rightarrow \cos \beta \epsilon H_h^*$)

$$\mathcal{N} = \begin{pmatrix} \left(\lambda_t^2 - \frac{g_3^2}{3} \right) \frac{s_c^2}{2} + \tilde{m}^2 & \lambda_t \tilde{B}_t \frac{s_c}{\sqrt{2}} \cos \beta & \lambda_t \tilde{A}_t \frac{s_c}{\sqrt{2}} \sin \beta \\ \lambda_t \tilde{B}_t \frac{s_c}{\sqrt{2}} \cos \beta & \tilde{m}^2 + \lambda_t^2 \frac{s_c^2}{2} \cos^2 \beta & \lambda_t^2 \frac{s_c^2}{4} \sin 2\beta \\ \lambda_t \tilde{A}_t \frac{s_c}{\sqrt{2}} \sin \beta & \lambda_t^2 \frac{s_c^2}{4} \sin 2\beta & \lambda_t^2 \frac{s_c^2}{2} \sin^2 \beta \end{pmatrix}, \quad (\text{A.6})$$

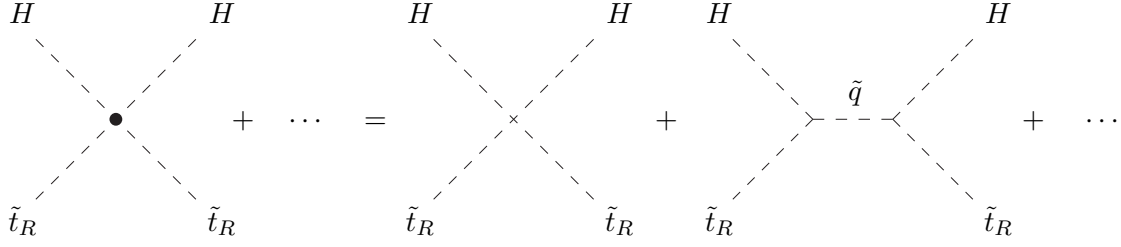


Figure 5: Tree-level proper vertex matching of Q .

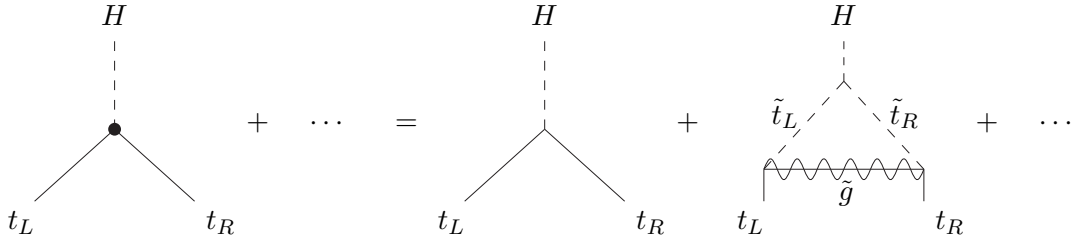


Figure 6: One-loop proper vertex matching of h_t at $\tau = \tilde{m}$.

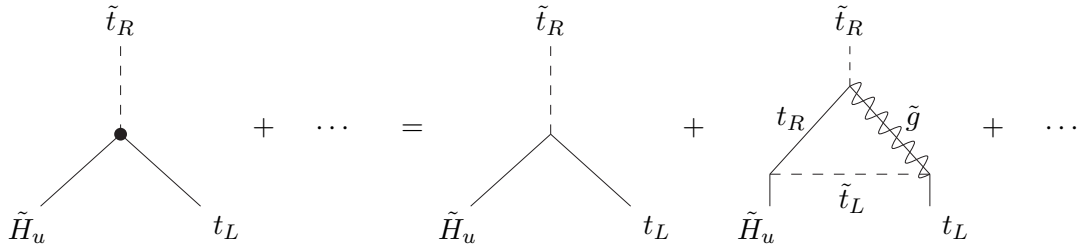


Figure 7: One-loop proper vertex matching of Y_t at $\tau = \tilde{m}$.

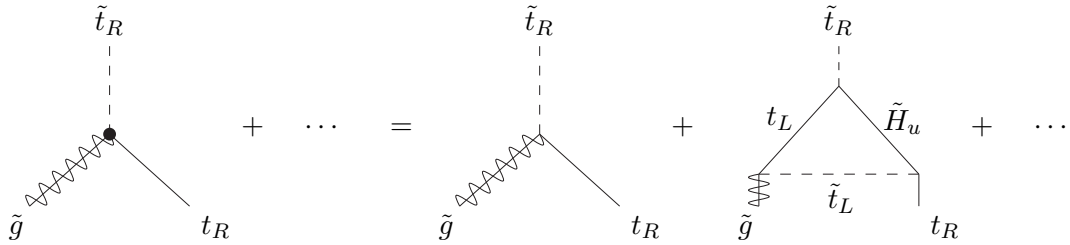


Figure 8: One-loop proper vertex matching of G at $\tau = \tilde{m}$.

$$\begin{array}{c} \tilde t_R \\ \bullet \end{array} \text{---} + \dots = \text{---} \tilde t_R + \tilde t_R \text{---} \left(\text{dashed circle} \right) \text{---} \tilde t_R + \tilde t_R \text{---} \left(\text{dashed circle} \right) \text{---} \tilde t_R + \dots$$

Figure 9: One-loop matching of the \tilde{t}_R wave function renormalization at $\tau = \tilde{m}$.

[illegible]

Figure 10: One-loop matching of the t_R wave function renormalization at $\tau = \tilde{m}$.

$$\begin{array}{c}
\begin{array}{ccccccc}
H(\tilde{t}_R) & & H(\tilde{t}_R) & & H(\tilde{t}_R) & & H(\tilde{t}_R) \\
& \diagdown & & \diagup & & \diagdown & & \diagup \\
& \bullet & & & & \times & & \\
& \diagup & & \diagdown & & \diagup & & \diagdown \\
H(\tilde{t}_R) & & H(\tilde{t}_R) & & H(\tilde{t}_R) & & H(\tilde{t}_R)
\end{array}
+
\begin{array}{c}
H(\tilde{t}_R) \quad \quad H(\tilde{t}_R) \\
\diagdown \quad \quad \diagup \\
\bullet \quad \quad \bullet \\
\diagup \quad \quad \diagdown \\
H(\tilde{t}_R) \quad \quad H(\tilde{t}_R)
\end{array}
\begin{array}{c}
\tilde{t}_R(H) \\
\text{---} \\
\tilde{t}_R(H)
\end{array}
+ \dots =
\begin{array}{c}
H(\tilde{t}_R) \quad \quad H(\tilde{t}_R) \\
\diagdown \quad \quad \diagup \\
\bullet \quad \quad \bullet \\
\diagup \quad \quad \diagdown \\
H(\tilde{t}_R) \quad \quad H(\tilde{t}_R)
\end{array}
\end{array}$$

$$\begin{array}{c}
\begin{array}{ccccccc}
H(\tilde{t}_R) & & H(\tilde{t}_R) & & H(\tilde{t}_R) & & H(\tilde{t}_R) \\
& \diagdown & & \diagup & & \diagdown & & \diagup \\
& \bullet & & & & \times & & \\
& \diagup & & \diagdown & & \diagup & & \diagdown \\
H(\tilde{t}_R) & & H(\tilde{t}_R) & & H(\tilde{t}_R) & & H(\tilde{t}_R)
\end{array}
+
\begin{array}{c}
H(\tilde{t}_R) \quad \quad H(\tilde{t}_R) \\
\diagdown \quad \quad \diagup \\
\bullet \quad \quad \bullet \\
\diagup \quad \quad \diagdown \\
H(\tilde{t}_R) \quad \quad H(\tilde{t}_R)
\end{array}
\begin{array}{c}
\tilde{t}_R(H) \\
\text{---} \\
\tilde{t}_R(H)
\end{array}
+
\begin{array}{c}
H(\tilde{t}_R) \quad \quad H(\tilde{t}_R) \\
\diagdown \quad \quad \diagup \\
\bullet \quad \quad \bullet \\
\diagup \quad \quad \diagdown \\
H(\tilde{t}_R) \quad \quad H(\tilde{t}_R)
\end{array}
\begin{array}{c}
\tilde{q} \\
\text{---} \\
\tilde{q}
\end{array}
+ \dots
\end{array}$$

Figure 11: One-loop proper vertex matching of $\lambda(K)$ at $\tau = \tilde{m}$.

with $\tilde{B}_t = A_t + \mu \tan \beta$, and finally $m_4^2 \equiv m_{q_1}^2 = m_5^2 \equiv m_{q_2}^2 = \tilde{m}^2 + \frac{s_c^2}{12}$. Extracting from the right-hand side of (A.5) the coefficient of the term $s_c^4/24$ we obtain ΔK as expressed in (A.12).

To conclude here we collect all the proper vertex thresholds

$$\Delta Q = -\lambda_t^2 \sin^2 \beta \frac{|\tilde{A}_t|^2}{\tilde{m}^2}, \quad (\text{A.7})$$

$$\Delta h_t = \frac{8}{3(4\pi)^2} g_3^2 \lambda_t \tilde{A}_t \sin \beta \, M_3 b_1 , \quad (\text{A.8})$$

$$\Delta G = \frac{2}{(4\pi)^2} g_3 \lambda_t^2 \left(-1 + \frac{\mu^2 \ln(\mu^2/\tilde{m}^2)}{\mu^2 - \tilde{m}^2} \right) , \quad (\text{A.9})$$

$$\Delta Y_t = \frac{8}{3(4\pi)^2} g_3^2 \lambda_t \left(1 - \frac{M_3^2 \ln(\tilde{m}^2/M_3^2)}{\tilde{m}^2 - M_3^2} \right) , \quad (\text{A.10})$$

$$\Delta \lambda = \frac{3}{8\pi^2} (\lambda_t \sin \beta)^4 \tilde{A}_t^4 \frac{\tilde{m}^2 - M_U^2 - M_U^2 \ln(\tilde{m}^2/M_U^2)}{(\tilde{m}^2 - M_U^2)^3} , \quad (\text{A.11})$$

$$\Delta K = c_0 + c_1 \frac{\tilde{A}_t}{\tilde{m}} + c_2 \frac{\tilde{A}_t^2}{\tilde{m}^2} + c_3 \frac{\tilde{A}_t^4}{\tilde{m}^4} , \quad (\text{A.12})$$

where

$$\begin{aligned} b_1 &= \frac{M_3^2(\tilde{m}^2 - M_U^2) \log(\tilde{m}^2/M_3^2) + M_U^2(\tilde{m}^2 - M_3^2) \log(\tilde{m}^2/M_U^2)}{(\tilde{m}^2 - M_3^2)(M_3^2 - M_U^2)(\tilde{m}^2 - M_U^2)} , \\ c_0 &= \frac{1}{16\pi^2} \left(3\lambda_t^4 \sin^2 2\beta + 2\lambda_t^2 \cos^2 \beta [g_3^2 - 3\lambda_t^2 (1 + \cos^2 \beta)] \frac{\tilde{B}_t^2}{\tilde{m}^2} + \lambda_t^4 \cos^4 \beta \frac{\tilde{B}_t^4}{\tilde{m}^4} \right) , \\ c_1 &= -\frac{3\lambda_t^4 \sin^2 2\beta \tilde{B}_t}{8\pi^2 \tilde{m}} , \\ c_2 &= \frac{1}{32\pi^2} \left(8\lambda_t^2 \sin^2 \beta [g_3^2 - 3\lambda_t^2 (1 - \sin^2 \beta)] + 3\lambda_t^4 \sin^2 2\beta \frac{\tilde{B}_t^2}{\tilde{m}^2} \right) , \\ c_3 &= -\frac{3\lambda_t^4 \sin^4 \beta}{4\pi^2} , \end{aligned}$$

along with the wave function threshold contributions of each external leg

$$\begin{aligned} Z_{\tilde{t}_R} &= 2 \left(\lambda_t \tilde{B}_t \cos \beta \right)^2 F(\tilde{m}^2) + 2 \left(\lambda_t \tilde{A}_t \cos \beta \right)^2 F(0) & [\tilde{q} H_h + \tilde{q} H], \\ Z_H &= \left(\lambda_t \tilde{A}_t \cos \beta \right)^2 F(M_U^2) & [\tilde{q} \tilde{t}_R], \\ Z_{t_R} &= 2 \left(\lambda_t \cos \beta \right)^2 E(0) + 2\lambda_t^2 E(\mu^2) & [H_h q + \tilde{q} \tilde{H}_u], \\ Z_{t_L} &= \left(\lambda_t \cos \beta \right)^2 E(0) + \frac{8}{3} g_3^2 E(M_3^2) & [H_h t_R + \tilde{q} \tilde{g}], \\ Z_{\tilde{H}_u} &= \lambda_t^2 E(0) & [\tilde{q} t_R], \\ Z_{\tilde{g}} &= 11 g_3^2 E(0) & [\tilde{q} q], \end{aligned} \quad (\text{A.13})$$

where the particles propagating in the loops are indicated inside squared brackets and the functions $F(m^2)$ and $E(m^2)$ are defined by

$$F(m^2) \equiv -\frac{1}{\tilde{m}^2(4\pi)^2} \frac{a^4 - 1 - 2a^2 \log(a^2)}{2(a^2 - 1)^3} , \quad (\text{A.14})$$

$$E(m^2) \equiv -\frac{1}{(4\pi)^2} \frac{-1 + (4 - 3a^2)a^2 + 2a^2 \log a^2}{4(a^2 - 1)^2} , \quad (\text{A.15})$$

with $a^2 = m^2/\tilde{m}^2$.

Because of the thresholds (A.13) the kinetic terms of the effective theory would not be canonically normalized if these wave function thresholds were not absorbed in a redefinition of the effective fields. This implies that any generic effective coupling ρ has also gotten a wave function threshold dependence coming from its field redefinitions as

$$1 - \frac{1}{2}\Delta Z_\rho \equiv 1 - \frac{1}{2}\sum_i Z_i \quad , \quad (\text{A.16})$$

where i runs over the fields of the interaction ρ .

A last remark concerns the gauge couplings. They have no threshold because Ward identities impose a cancellation between the proper vertex threshold and the non-vector fields wave function ones. Therefore a possible threshold could only come from the vector boson wave function threshold but the latter is zero when evaluated at the renormalization scale \tilde{m} . Finally let us observe that the mass thresholds are not necessary for our aim. In fact the LE masses only appear inside one-loop thresholds in which a possible one-loop mass thresholds would only contribute at two-loop.

Finally if we assume the gluino mass heavy enough (but below \tilde{m}), it is necessary to also integrate it out and repeat at the scale $\tau = M_3$ the procedure just described. The gluino decoupling affects the proper vertex K and the right-handed top and stop propagators, which produce the right-handed top and stop wave function thresholds and the mass threshold $\Delta' M_U^2$ ⁷.

Concerning the wave function thresholds, the matching conditions at $\tau = M_3$ lead to

$$\begin{aligned} \Delta' Z_{t_R} &= \frac{5 G^2}{6(4\pi)^2} \quad , \\ \Delta' Z_{\tilde{t}_R} &= \frac{2 G^2}{3(4\pi)^2} \frac{3 - 4b^2 + b^4 - 2b^2(b^2 - 2) \log b^2}{(b^2 - 1)^2} \quad , \end{aligned} \quad (\text{A.17})$$

where $b^2 = M_U^2/M_3^2$.

In order to calculate the proper vertex threshold $\Delta' K$ and $\Delta' M_U^2$ we use the procedure of matching the stop effective potential in the presence of a background field. After giving a VEV to the third colour stop, $\langle \tilde{t}_{R3} \rangle = s_c/\sqrt{2}$, mixing mass terms between right top and gluino are generated but, after diagonalizing, only $t_R^{(3)}$ and $\tilde{g}^{(8)}$ have masses depending on s_c ; explicitly $r_\pm = M_3 \pm \sqrt{G^2 s_c^2 4/3 + M_3^2}$. Therefore the thresholds can come only from the contribution to the effective potential of the heaviest fermionic eigenstate, which results

$$-\frac{2r_+^4}{64\pi^2} \left[\log \frac{r_+^2}{M_3^2} - \frac{3}{2} \right] = \frac{3 M_3^4}{64\pi^2} + \frac{G^2 M_3^2}{24\pi^2} s_c^2 - \frac{G^4}{144\pi^2} s_c^4 + \mathcal{O}(s_c^6) \quad , \quad (\text{A.18})$$

⁷We also consider the mass thresholds because we want to know the masses evolution beyond the decoupling scale M_3 .

and thus

$$\begin{aligned}\Delta' K &= -\frac{G^4}{6\pi^2} , \\ \Delta' M_3 &= \frac{G^2 M_3^2}{24\pi^2} .\end{aligned}\tag{A.19}$$

B RENORMALIZATION GROUP EQUATIONS

In this appendix we sketch the calculation of the one-loop RGE in the ET ⁸. In order to present our result it is useful to define

$$\beta_\eta \equiv \frac{\partial \eta}{\partial \ln \tau} = \beta_\eta^{(v)} + \eta \sum_i \frac{n_i}{2} \gamma_{\rho_i} , \tag{B.1}$$

where τ is the renormalization scale, η is the coupling between different fields ρ_i with multiplicity n_i where the index i runs over the fields which are involved in the particular vertex, and the functions $\beta_\eta^{(v)}$ and $\eta \gamma_{\rho_i}$ are the respective contributions from the renormalization of the proper vertex and the anomalous dimension of each external leg. In the same way as for the threshold effects the β_η and γ_{ρ_i} functions are computed in the \overline{MS} renormalization scheme and using the Landau gauge. We will implicitly consider renormalization scales τ larger than any fermionic mass, in particular the gluino mass M_3 , and for $\tau < M_3$ the correct results are obtained by simply erasing the couplings G and M_3 and disregarding $\beta_{\tilde{g}}$ and $\gamma_{\tilde{g}}$.

By using the diagrammatic procedure we find

$$\begin{aligned}(4\pi)^2 \gamma_{\tilde{t}_R} &= 4Y_t^2 + \frac{16}{3}G^2 - 8g_3^2 , \\ (4\pi)^2 \gamma_{q_L} &= h_t^2 + Y_t^2 , \\ (4\pi)^2 \gamma_{t_R} &= 2h_t^2 + \frac{8}{3}G^2 , \\ (4\pi)^2 \gamma_H &= 6h_t^2 , \\ (4\pi)^2 \gamma_{\tilde{H}_u} &= 3Y_t^2 , \\ (4\pi)^2 \gamma_{\tilde{g}} &= G^2 . \\ \gamma_{\tilde{W}} &= \gamma_{\tilde{B}} = \gamma_{\tilde{H}_d} = 0\end{aligned}\tag{B.2}$$

and

$$\begin{aligned}\beta_{g_u}^{(v)} &= \beta_{g'_u}^{(v)} = \beta_{g_d}^{(v)} = \beta_{g'_d}^{(v)} = \beta_J^{(v)} = \beta_{Y_t}^{(v)} = 0 , \\ (4\pi)^2 \beta_G^{(v)} &= -9 g_3^2 G , \\ (4\pi)^2 \beta_{h_t}^{(v)} &= -8 h_t g_3^2 .\end{aligned}\tag{B.3}$$

⁸We have checked that our results are consistent with the MSSM [21] and Split Supersymmetry [18] limits.

On the other hand to compute $\beta_\lambda^{(v)}$, $\beta_Q^{(v)}$ and $\beta_K^{(v)}$ we have found it very convenient to use the effective potential method [31]. In order to do that we introduce background fields ϕ_c and s_c for H and \tilde{t}_R defined as

$$H \rightarrow 1/\sqrt{2} \begin{pmatrix} \phi_2 + i\phi_3 \\ h + \phi_c + i\phi_1 \end{pmatrix} \quad (\text{B.4})$$

$$\tilde{t}_R^{(\omega)} \rightarrow 1/\sqrt{2} \left(\tilde{t}_{1R}^{(\omega)} + \delta^{j3} s_c + i\tilde{t}_{2R}^{(\omega)} \right), \quad (\text{B.5})$$

where ω is the color index. In this background some fields acquire a mass and, in particular, the bosonic mass spectrum becomes

$$\begin{aligned} g^a : & \quad m^2 = 0 & a = 1, 2, 3 \\ g^a : & \quad m^2 = s_c^2 g_3^2/4 & a = 4, 5, 6, 7 \\ g^a : & \quad m^2 = s_c^2 g_3^2/3 & a = 8 \\ \phi_\omega : & \quad m^2 = \phi_c^2 \lambda/2 + s_c^2 Q/2 & \omega = 1, 2, 3 \\ \tilde{t}_{1R}^{(\omega)}, \tilde{t}_{2R}^{(\alpha)} : & \quad m^2 = \phi_c^2 Q/2 + s_c^2 K/6 & \omega = 1, 2, 3 \quad \alpha = 1, 2 \\ \begin{pmatrix} \tilde{t}_{1R}^{(3)} \\ h \end{pmatrix} : & \quad m^2 = \frac{1}{2} \begin{pmatrix} s_c^2 K + \phi_c^2 Q & 2s_c \phi_c Q \\ 2s_c \phi_c Q & 3\phi_c^2 \lambda + s_c^2 Q \end{pmatrix} \end{aligned} \quad (\text{B.6})$$

where we have written only the terms which depend on ϕ_c and/or s_c . Analogously the fermionic mass spectrum looks like

$$\begin{pmatrix} b_L^{(3)} \\ \tilde{H}_u^+ \end{pmatrix} : m = \begin{pmatrix} 0 & Y' \\ Y' & 0 \end{pmatrix} \quad (\text{B.7})$$

$$\begin{pmatrix} t_L^{(1)} \\ t_R^{(1)\dagger} \\ g^{(4)} \\ g^{(5)} \end{pmatrix} : m = \begin{pmatrix} 0 & h' & 0 & 0 \\ h' & 0 & G' & -iG' \\ 0 & G' & 0 & 0 \\ 0 & -iG' & 0 & 0 \end{pmatrix} \quad (\text{B.8})$$

$$\begin{pmatrix} t_L^{(2)} \\ t_R^{(2)\dagger} \\ g^{(6)} \\ g^{(7)} \end{pmatrix} : m = \begin{pmatrix} 0 & h' & 0 & 0 \\ h' & 0 & G' & -iG' \\ 0 & G' & 0 & 0 \\ 0 & -iG' & 0 & 0 \end{pmatrix} \quad (\text{B.9})$$

$$\begin{pmatrix} t_L^{(3)} \\ t_R^{(3)\dagger} \\ \tilde{H}_u^0 \\ g^{(8)} \end{pmatrix} : m = \begin{pmatrix} 0 & h' & Y' & 0 \\ h' & 0 & 0 & -\frac{2G'}{\sqrt{3}} \\ Y' & 0 & 0 & 0 \\ 0 & -\frac{2G'}{\sqrt{3}} & 0 & 0 \end{pmatrix} \quad (\text{B.10})$$

where $h' = \phi_c h_t / \sqrt{2}$, $Y' = s_c Y_t / \sqrt{2}$ and $G' = s_c G / 2$.

Using the property of invariance of the effective potential with respect to the renormalization scale we can write

$$\begin{aligned} \tau \frac{dV(\phi_c, s_c)}{d\tau} = \\ \tau \frac{d}{d\tau} \left(V_0(\phi_c, s_c) + \frac{1}{64\pi^2} \text{STr} \left[\mathcal{M}^4(\phi_c, s_c) \ln \left[\frac{\mathcal{M}^4(\phi_c, s_c)}{\tau^2} \right] \right] + \dots \right) \\ = \dots + \frac{1}{8} \beta_\lambda^{(v)} \phi_c^4 + \frac{1}{24} \beta_K^{(v)} s^4 + \frac{1}{4} \beta_Q^{(v)} \phi_c^2 s_c^2 - \frac{1}{32\pi} \text{STr} [\mathcal{M}^4(\phi_c, s_c)] = 0 , \end{aligned} \quad (\text{B.11})$$

where the ellipses stand for terms we are not interested in, $V_0(\phi_c, s_c)$ is the tree-level scalar potential of (2.1) in the presence of the background fields ϕ_c and s_c , $\mathcal{M}^2(\phi_c, s_c)$ is the mass spectrum of the fields written in (B.6)-(B.10) and, finally, for a given function $f(\mathcal{M}^2)$ of the squared mass matrix of all fields in the theory, $\text{STr} f(\mathcal{M}^2) \equiv \text{Tr} \sum_J (-1)^{2J} (2J+1) f(\mathcal{M}_J^2)$. Therefore in (B.11) $\beta_\lambda^{(v)}$, $\beta_Q^{(v)}$ and $\beta_K^{(v)}$ are put easily in evidence by the expansion in powers of s_c and ϕ_c of $\text{STr} \mathcal{M}^4(\phi_c, s_c)$. Furthermore for our purposes only the terms $M_J^4(\phi_c, s_c)$ proportional to s_c^4 , ϕ_c^4 or $s_c^2 \phi_c^2$ are interesting and consequently we can ignore in $M_J^2(\phi_c, s_c)$ the dependence on dimensional couplings, as we have done in (B.6)-(B.10). After performing the corresponding expansions we get the β -functions

$$\begin{aligned} (4\pi)^2 \beta_\lambda^{(v)} &= 12\lambda^2 + 6Q^2 - 12h_t^4 , \\ (4\pi)^2 \beta_Q^{(v)} &= KQ + 3\lambda Q + 4Q^2 - \frac{32}{3} G^2 h_t^2 - 4Y_t^2 h_t^2 , \\ (4\pi)^2 \beta_K^{(v)} &= 12Q^2 + \frac{14}{3} K^2 + 13g_3^4 - \frac{88}{3} G^4 - 24Y_t^4 . \end{aligned} \quad (\text{B.12})$$

Finally by plugging the results (B.2), (B.3) and (B.12) into (B.1), we find the result which was anticipated in (2.12).

In order to complete our renormalization picture we will compute now the running of the masses. By using standard diagrammatic methods we obtain

$$\begin{aligned} \beta_{M_1}^{(v)} &= \beta_{M_2}^{(v)} = \beta_\mu^{(v)} = 0 , \\ (4\pi)^2 \beta_{M_3}^{(v)} &= -18g_3^2 M_3 , \\ (4\pi)^2 \beta_{m^2}^{(v)} &= -6Q m_U^2 , \\ (4\pi)^2 \beta_{M_U^2}^{(v)} &= -\frac{32}{3} M_3^2 G^2 + \frac{8}{3} K M_U^2 - 4m^2 Q - 4Y_t^2 \mu^2 , \end{aligned} \quad (\text{B.13})$$

and using (B.1) and (B.2) we find the expressions in Eq. (2.13).

References

- [1] V. A. Kuzmin, V. A. Rubakov and M. E. Shaposhnikov, Phys. Lett. B **155**, 36 (1985); A. G. Cohen, D. B. Kaplan and A. E. Nelson, Nucl. Phys. B **349**, 727 (1991); M. Joyce, T. Prokopec and N. Turok, Phys. Lett. B **339** (1994) 312;

- M. Quiros, *Helv. Phys. Acta* **67**, 451 (1994); *Acta Phys. Polon. B* **38**, 3661 (2007); V. A. Rubakov and M. E. Shaposhnikov, *Usp. Fiz. Nauk* **166**, 493 (1996) [*Phys. Usp.* **39**, 461 (1996)] [arXiv:hep-ph/9603208]; M. S. Carena and C. E. M. Wagner, arXiv:hep-ph/9704347; A. Riotto and M. Trodden, *Ann. Rev. Nucl. Part. Sci.* **49**, 35 (1999) [arXiv:hep-ph/9901362].
- [2] M. E. Shaposhnikov, *Nucl. Phys. B* **287**, 757 (1987).
- [3] M. B. Gavela, P. Hernandez, J. Orloff and O. Pene, *Mod. Phys. Lett. A* **9** (1994) 795 [arXiv:hep-ph/9312215]; *Nucl. Phys. B* **430**, 382 (1994) [arXiv:hep-ph/9406289]; P. Huet and E. Sather, *Phys. Rev. D* **51**, 379 (1995) [arXiv:hep-ph/9404302].
- [4] G. F. Giudice, *Phys. Rev. D* **45**, 3177 (1992); S. Myint, *Phys. Lett. B* **287**, 325 (1992) [arXiv:hep-ph/9206266].
- [5] J. R. Espinosa, M. Quiros and F. Zwirner, *Phys. Lett. B* **307**, 106 (1993) [arXiv:hep-ph/9303317]; A. Brignole, J. R. Espinosa, M. Quiros and F. Zwirner, *Phys. Lett. B* **324**, 181 (1994) [arXiv:hep-ph/9312296].
- [6] M. S. Carena, M. Quiros and C. E. M. Wagner, *Phys. Lett. B* **380**, 81 (1996) [arXiv:hep-ph/9603420]; D. Delepine, J. M. Gerard, R. Gonzalez Felipe and J. Weyers, *Phys. Lett. B* **386**, 183 (1996) [arXiv:hep-ph/9604440]; M. S. Carena, M. Quiros and C. E. M. Wagner, *Nucl. Phys. B* **524**, 3 (1998) [arXiv:hep-ph/9710401].
- [7] S. J. Huber, *JCAP* **0602**, 008 (2006) [arXiv:hep-ph/0508208].
- [8] M. Pietroni, *Nucl. Phys. B* **402**, 27 (1993) [arXiv:hep-ph/9207227]; S. J. Huber and M. G. Schmidt, *Nucl. Phys. B* **606**, 183 (2001) [arXiv:hep-ph/0003122].
- [9] A. Menon, D. E. Morrissey and C. E. M. Wagner, *Phys. Rev. D* **70**, 035005 (2004) [arXiv:hep-ph/0404184]; S. J. Huber, T. Konstandin, T. Prokopec and M. G. Schmidt, *Nucl. Phys. B* **757**, 172 (2006) [arXiv:hep-ph/0606298]; C. Balazs, M. S. Carena, A. Freitas and C. E. M. Wagner, *JHEP* **0706**, 066 (2007) [arXiv:0705.0431 [hep-ph]].
- [10] J. Kang, P. Langacker, T. j. Li and T. Liu, *Phys. Rev. Lett.* **94**, 061801 (2005) [arXiv:hep-ph/0402086].
- [11] M. Carena, M. Quiros, A. Riotto, I. Vilja and C. E. M. Wagner, *Nucl. Phys. B* **503**, 387 (1997); J. M. Cline and K. Kainulainen, *Phys. Rev. Lett.* **85**, 5519 (2000) [arXiv:hep-ph/0002272]; J. M. Cline, M. Joyce and K. Kainulainen, *JHEP* **0007**, 018 (2000) [arXiv:hep-ph/0006119]; M. S. Carena, J. M. Moreno, M. Quiros, M. Seco and C. E. M. Wagner, *Nucl. Phys. B* **599**, 158 (2001) [arXiv:hep-ph/0011055]; M. S. Carena, M. Quiros, M. Seco and C. E. M. Wagner, *Nucl. Phys. B* **650**, 24 (2003) [arXiv:hep-ph/0208043]. T. Konstandin, T. Prokopec, M. G. Schmidt and M. Seco, *Nucl. Phys. B* **738**, 1 (2006) [arXiv:hep-ph/0505103]; V. Cirigliano, S. Profumo and M. J. Ramsey-Musolf, *JHEP* **0607**, 002 (2006) [arXiv:hep-ph/0603246].

- [12] D. J. H. Chung, B. Garbrecht, M. J. Ramsey-Musolf and S. Tulin, arXiv:0808.1144 [hep-ph].
- [13] M. Carena, G. Nardini, M. Quiros and C. E. M. Wagner, arXiv:0809.3760 [hep-ph].
- [14] D. Chang, W. Y. Keung and A. Pilaftsis, Phys. Rev. Lett. **82**, 900 (1999) [Erratum-ibid. **83**, 3972 (1999)] [arXiv:hep-ph/9811202].
- [15] B. C. Regan, E. D. Commins, C. J. Schmidt and D. DeMille, Phys. Rev. Lett. **88**, 071805 (2002); S. Abel, S. Khalil and O. Lebedev, Nucl. Phys. B **606**, 151 (2001) [arXiv:hep-ph/0103320].
- [16] C. Balazs, M. S. Carena and C. E. M. Wagner, Phys. Rev. D **70**, 015007 (2004) [arXiv:hep-ph/0403224]; C. Balazs, M. S. Carena, A. Menon, D. E. Morrissey and C. E. M. Wagner, Phys. Rev. D **71**, 075002 (2005) [arXiv:hep-ph/0412264].
- [17] H. Georgi, Ann. Rev. Nucl. Part. Sci. **43**, 209 (1993).
- [18] N. Arkani-Hamed and S. Dimopoulos, JHEP **0506**, 073 (2005) [arXiv:hep-th/0405159]; G. F. Giudice and A. Romanino, Nucl. Phys. B **699**, 65 (2004) [Erratum-ibid. B **706**, 65 (2005)] [arXiv:hep-ph/0406088].
- [19] W. M. Yao *et al.* [Particle Data Group], “Review of particle physics,” J. Phys. G **33**, 1 (2006).
- [20] M. E. Machacek and M. T. Vaughn, Nucl. Phys. B **222**, 83 (1983); M. E. Machacek and M. T. Vaughn, Nucl. Phys. B **236**, 221 (1984); M. E. Machacek and M. T. Vaughn, Nucl. Phys. B **249**, 70 (1985).
- [21] S. P. Martin and M. T. Vaughn, Phys. Rev. D **50**, 2282 (1994) [arXiv:hep-ph/9311340].
- [22] M. S. Carena, S. Pokorski and C. E. M. Wagner, Nucl. Phys. B **406**, 59 (1993) [arXiv:hep-ph/9303202].
- [23] P. Langacker and N. Polonsky, Phys. Rev. D **47**, 4028 (1993) [arXiv:hep-ph/9210235].
- [24] A. C. Kraan, arXiv:hep-ex/0305051.
- [25] T. Aaltonen *et al.* [CDF Collaboration], Phys. Rev. D **76**, 072010 (2007) [arXiv:0707.2567 [hep-ex]].
- [26] V. M. Abazov *et al.* [D0 Collaboration], arXiv:0803.2263 [hep-ex].
- [27] S. Kraml and A. R. Raklev, Phys. Rev. D **73**, 075002 (2006) [arXiv:hep-ph/0512284]; AIP Conf. Proc. **903**, 225 (2007) [arXiv:hep-ph/0609293].
- [28] M. Carena, A. Freitas and C. E. M. Wagner, arXiv:0808.2298 [hep-ph].

- [29] M. S. Carena, A. Menon, R. Noriega-Papaqui, A. Szyrkman and C. E. M. Wagner, Phys. Rev. D **74**, 015009 (2006) [arXiv:hep-ph/0603106].
- [30] M. S. Carena, J. R. Espinosa, M. Quiros and C. E. M. Wagner, Phys. Lett. B **355**, 209 (1995) [arXiv:hep-ph/9504316]; M. S. Carena, M. Quiros and C. E. M. Wagner, Nucl. Phys. B **461**, 407 (1996) [arXiv:hep-ph/9508343]; S. Heinemeyer, W. Hollik, and G. Weiglein, Phys. Rev. D **58**, 091701 (1998) [arXiv:hep-ph/9803277]; S. Heinemeyer, W. Hollik, and G. Weiglein, Phys. Lett. B **440**, 296 (1998) [arXiv:hep-ph/9807423]; S. Heinemeyer, W. Hollik, and G. Weiglein, Eur. Phys. J. C **9**, 343 (1999) [arXiv:hep-ph/9812472]; J. R. Espinosa and R. J. Zhang, J. High Energy Phys. **0003**, 026 (2000) [arXiv:hep-ph/9912236]; J. R. Espinosa and R. J. Zhang, Nucl. Phys. B **586**, 3 (2000) [arXiv:hep-ph/0003246]; M. Carena, H. E. Haber, S. Heinemeyer, W. Hollik, C. E. M. Wagner, and G. Weiglein, Nucl. Phys. B **580**, 29 (2000) [arXiv:hep-ph/0001002]; G. Degrandi, P. Slavich, and F. Zwirner, Nucl. Phys. B **611**, 403 (2001) [arXiv:hep-ph/0105096]; A. Brignole, G. Degrandi, P. Slavich, and F. Zwirner, arXiv:hep-ph/0112177; S. P. Martin, Phys. Rev. D **67**, 095012 (2003) [arXiv:hep-ph/0211366].
- [31] B. Gato, J. Leon, J. Perez-Mercader and M. Quiros, Nucl. Phys. B **253**, 285 (1985).